ADVANCED OPTICAL MATERIALS
www.advopticalmat.de

Persistent Luminescence Induced by Upconversion: An Alternative Approach for Rechargeable Bio-Emitters

Luidgi Giordano, Guanyu Cai, Johanne Seguin, Jianhua Liu, Cyrille Richard, Lucas Carvalho Veloso Rodrigues,* and Bruno Viana**

The charging of persistent luminescence using an infrared laser as a power source and an upconversion process is a recently proposed trend in the field of persistent luminescence that allows expansion of the potential applications for these materials. In bioimaging at nanoscale, it allows for increased rechargeability capacity, as the excitation wavelength is fully inside the biological window. In this work, a novel approach is proposed to this phenomenon using energy transfer on associated materials. For this purpose, β-$NaGd_{0.8}Yb_{0.17}Er_{0.03}F_4$ nanoparticles, known for their efficient upconversion, and $Zn_{1.33}Ga_{1.335}Sn_{0.33}Cr_{0.005}O_4$ nanoparticles, known for their persistent luminescence properties, have been synthesized and associated through a dry impregnation method. The obtained hybrid material is found to present persistent luminescence at 700 nm after charging with a 980 nm laser. A mechanism is proposed to explain this energy transfer process and the capabilities of the hybrid material as rechargeable persistent nanoprobe for in vivo applications are shown.

1. Introduction

Persistent luminescence is an optical phenomenon in which luminescence is still ongoing for a long time after the end of excitation, lasting from minutes to hours.[1] The first persistent luminescence material was reported in the 17th century by Cascariolo, after he synthesized what is now known as the Bologna stone, and later shown by Lastusaari et al. to be $BaS:Cu^+$, originated from the calcination of $BaSO_4$ found in Paderno.[2] But even earlier, usages of these materials can be found in history, such as in ancient China.[3]

Modern studies on persistent luminescence were reignited during the 1990s, with a report of a long-lasting persistent material, $SrAl_2O_4:Eu^{2+}$, Dy^{3+} by Matsuzawa et al.[4] Since then the field has rapidly grown, with reports of dozens of persistent materials by many groups around the world,[3,5–12] and growing applications, from toys, luminous watches, and safety signs to in vivo and in vitro imaging, theranostics and therapy.[3,13–17]

The mechanisms for persistent luminescence usually involve the absorption of a high energy excitation source, such as X-rays, UV, or visible light, for storage of electrons or holes in defects in the crystal structure, either locally around the luminescent center, or in defects over the lattice.[18] These trapped electrons/holes are then released by thermal energy, and recombined into ground state, with radiative emission.[1,3,11,16,19,20]

In recent years, some studies using upconversion (i.e., emission of a photon with a smaller wavelength than the excitation source) as a way to charge the persistent materials have been introduced using different approaches. So far, three mechanisms have been unveiled (**Scheme 1**). These mechanisms are: i) phonon assisted direct charging of a low-energy level of the persistent luminescent centers, as shown for $Zn_3Ga_2GeO_8:Cr^{3+}$,[21] $ZnGa_2O_4:Cr^{3+}$,[22] $LiGa_5O_8:Cr^{3+}$, $MgGeO_3:Mn^{2+}$, and $MgGeO_3:Pr^{3+}$;[23] ii) introduction of an upconversion pair (Yb/Er; Yb/Tm; Yb/Ho) together with the persistent luminescent emission center[24] in matrices such as $Zn_3Ga_2GeO_8:Yb^{3+}$, Er^{3+}, Cr^{3+},[24] or $ZnGa_2O_4:Yb^{3+}$, Er^{3+}, Cr^{3+};[25] and iii) radiative energy transfer between UCNPs (upconversion nanoparticles) and PLNPs (persistent luminescent nanoparticles), with reported systems of $NaYF_4$:20%Yb, 2%Er@$NaYF_4$ UCNPs transferring to CaS:0.02%Eu,0.1%Tm,0.1%Ce PLNPs[26] and $NaYF_4$:20%Yb,1%Tm transferring to three different persistent luminescent materials.[27] Although a core–shell system would be ideal to work with by limiting the losses caused by longer distances between donors and acceptors in the upconversion persistent luminescence (UCPL) mechanism, hitherto there are no available works in the literature that successfully synthesized such oxide/fluoride composite.

L. Giordano, L. C. V. Rodrigues
Department of Fundamental Chemistry
Institute of Chemistry
University of São Paulo
Av. Prof. Lineu Prestes 748, São Paulo–SP CEP 05508-000, Brazil
E-mail: lucascvr@iq.usp.br

L. Giordano, G. Cai, B. Viana
Institut de Recherche de Chimie Paris
Chimie ParisTech – CNRS
PSL Research University
Paris 75005, France
E-mail: bruno.viana@chimie-paristech.fr

G. Cai, J. Seguin, J. Liu, C. Richard
Unité de Technologies Chimiques et Biologiques pour la Santé (UTCBS)
CNRS (UMR 8258) - U1267 INSERM
Faculté de Pharmacie
Université Paris Cité
Paris 75006, France
E-mail: cyrille.richard@u-paris.fr

The ORCID identification number(s) for the author(s) of this article can be found under https://doi.org/10.1002/adom.202201468.

DOI: 10.1002/adom.202201468

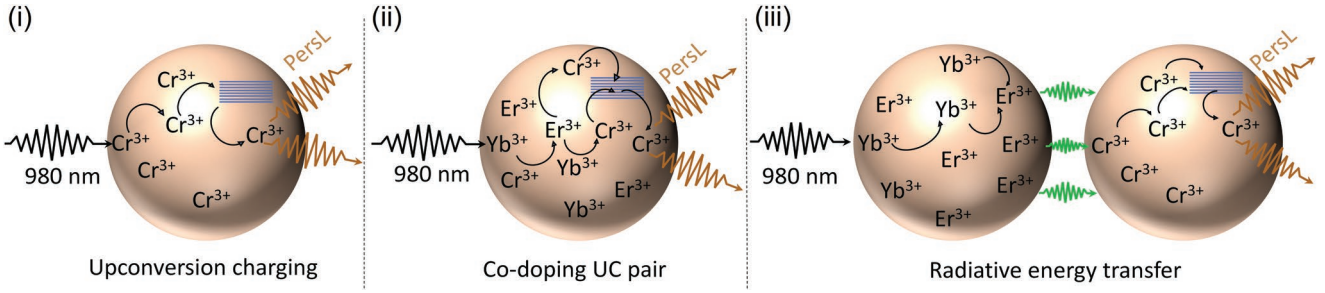

Scheme 1. i,ii) Different upconverted persistent luminescence (UCPL) approaches in the literature, taking Cr^{3+} as recombination center and Yb^{3+}, Er^{3+} as upconversion pair. iii) Schematic of the present work.

In this paper, we present new inputs on the upconversion capabilities toward persistent luminescence phenomenon associating $NaGdF_4$:17%Yb^{3+}, 3%Er^{3+} nanoparticles, considered as one of the best upconverting materials available and $Zn_{1.33}Ga_{1.335}Sn_{0.33}Cr_{0.005}O_4$ (ZGSO), a $ZnGa_2O_4$:Cr^{3+} (ZGO) derivative, which was synthesized as nanoparticles for the first time in the present work. Both matrices were intimately mixed using dry impregnation to associate ZGSO with β-$NaGdF_4$:Yb^{3+}, Er^{3+}. Further, we propose a mechanism for the upconverted persistent luminescence (UCPL) of this system and propose applications in bioimaging for this composite.

2. Results and Discussion

In comparison to other previous systems developed for UCPL, the combination of ZGSO and $NaGdF_4$ is advantageous for several reasons. i) As stated before, both are well established materials in regard to their efficiency in persistent luminescence and upconversion, respectively.[28,29] ii) Additionally, both have already been studied for in vitro or in vivo imaging separately, with good results and no safety problems.[13,30–34] iii) The proposed system has both excitation and emission wavelengths falling inside the biological window (BW-I),[35] leading to a potential in vivo rechargeable persistent luminescence probe excited by upconversion. iv) The process used (impregnation method) allows the proportion of each material to be adjusted easily and rapidly in the composite.

X-ray diffraction patterns for both materials prepared separately are available in Figures S1 and S2 (Supporting Information). In both cases, no phase impurity was found.

ZGSO NPs were synthesized for the first time using a hydrothermal method derived from the already well known ZGO synthesis developed in our research groups.[13,36] Compared to ZGO, already a remarkable material for persistent luminescence in the deep red,[37–39] ZGSO presents higher visible excitation efficiency for persistent luminescence and improved performance in the initial times of the persistent luminescence decay.[28] The high excitation capability of persistent luminescence in the visible range renders ZGSO among the best material able to efficiently store energy using Er^{3+} upconverted emission. The average size of ZGSO particles in TEM is ≈40 nm, as reported in **Figure 1**a.

$NaGdF_4$:Yb^{3+}, Er^{3+} is a well-known material with high efficiency upconversion feature due to low phonon energy of the fluoride host preventing non-radiative relaxation. This compound was synthesized by a co-precipitation method adapted from Palo et al.[40] The obtained nanoparticles have an average size of 15 nm. (Figure 1b).

Transmission electron microscopy (TEM) images for these associated particles obtained by dry impregnation can be seen in Figure 1c,d. Sphere-like shapes, with sizes ≈15–20 nm, correspond to the $NaGdF_4$ hexagonal-phase. The bigger size squares correspond to the ZGSO spinel nanoparticles. Then within this work, we present an easy method to associate the two nanoparticles that can be proposed to the end-users.

The optical spectroscopic features of the materials were studied both separately and after the association. For the upconverting material, the emission spectrum using a 980 nm laser diode as excitation can be seen in Figure 1e. It shows both common transitions reported in Yb, Er upconversion systems, the green $^2H_{11/2}$,$^4S_{3/2} \rightarrow {}^4I_{15/2}$ transitions and the red $^4F_{9/2} \rightarrow {}^4I_{15/2}$ transition. Notice that the blue $^2H_{9/2} \rightarrow {}^4I_{15/2}$ transition is not observed here. The power law dependence (Figure S4, Supporting Information) shows that as expected more than one photon is involved in both emissions, with slope being 1.93 for the green emission, and 1.65 for the red one, in good agreement with the already reported power law dependence for this system.[41–43]

For the persistent luminescent material, the more intensive emission band at ca. 700 nm is attributed to the radiative spin forbidden $^2E \rightarrow {}^4A_2$ transition. A tail beyond 750 nm was attributed to the small contribution of the $^4T_2 \rightarrow {}^4A_2$ transition in thermal equilibrium.[44] The excitation spectrum of ZGSO's photoluminescence considering its emission at 700 nm (Figure 1f, black line) shows two broad bands in the visible range, that can be attributed to the $^4A_2 \rightarrow {}^4T_2$ (≈570 nm) and $^4A_2 \rightarrow {}^4T_1$ (^4F) (≈420 nm) transitions. The third band in the UV (<350 nm) is attributed to the $^4A_2 \rightarrow {}^4T_1$ (^4P) transition partially overlapping the bandgap absorption. The $^4A_2 \rightarrow {}^4T_2$ excitation band is in good resonance with the Er^{3+} emission ($^2H_{11/2}$,$^4S_{3/2} \rightarrow {}^4I_{15/2}$ transitions), as there is an overlap between the two transitions (**Figure 2**a, red line). In the first step, to analyze if the green emission coming from erbium can promote persistent luminescence, a 565 nm LED that well corresponds to the green upconversion from erbium was used. Additionally, to compare with data obtained from micrometric powder in the literature, a 254 nm excitation light was used for the sake of comparison. The photoluminescence spectra are shown in Figure 2b. The emission spectra are similar for both excitation wavelengths and are also in well agreement with the data reported for micrometric size ZGSO, with the N2 line at

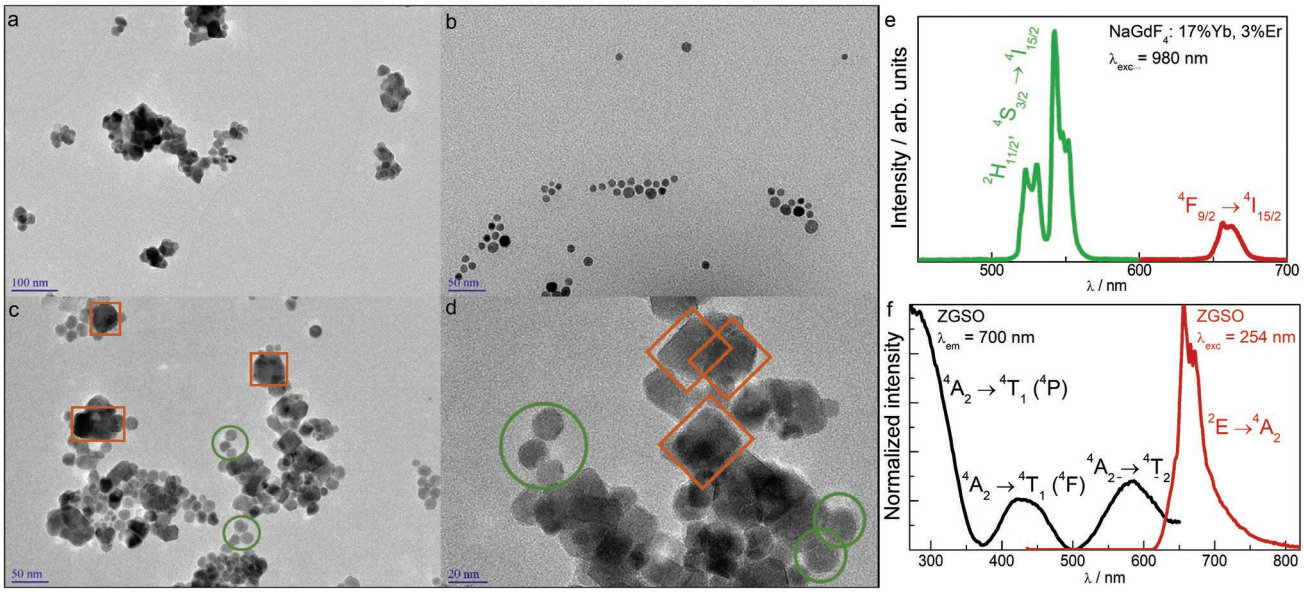

Figure 1. a) TEM image of ZGSO. b) TEM image of $NaGdF_4$:Yb, Er. c,d) TEM images of $NaGdF_4$:Yb^{3+}, Er^{3+} mixed with ZGSO:Cr^{3+} obtained by dry impregnation. ZGSO particles are indicated by orange squares, and $NaGdF_4$ particles by green circles. e) Upconversion spectrum for $NaGdF_4$:17%Yb^{3+}, 3% Er^{3+} nanoparticles after excitation at 980 nm. f) Excitation (λ_{em} = 700 nm) and emission (λ_{exc} = 254 nm) spectra of ZGSO.

ca. 694 nm enlarged and enhanced as a consequence of Sn^{4+} doping in regards to the ZGO:Cr matrix, a slight modification of the crystal field due to the cationic substitution.[28] Notice that the enhancement of the N2/R1 ratio is favorable to the persistent luminescence properties[45] as presented in Figure S5 (Supporting Information).

The persistent luminescence spectra are shown in Figure 2c with a 5 min charging time under 565 and 980 nm excitation, and 2 min for 254 nm excitation. It was previously demonstrated that in persistent phosphors: charging time, wavelengths and temperatures are very important parameters.[46,47] As the efficiency of the UV charging is much higher, the spectrometer slits are, 0.1 and 1 mm for 254 and 565 nm, respectively. This leads to experimental spectral broadening as seen in Figure 2c for the 565 nm excitation. The most prominent band in the persistent luminescence spectrum under 254 nm

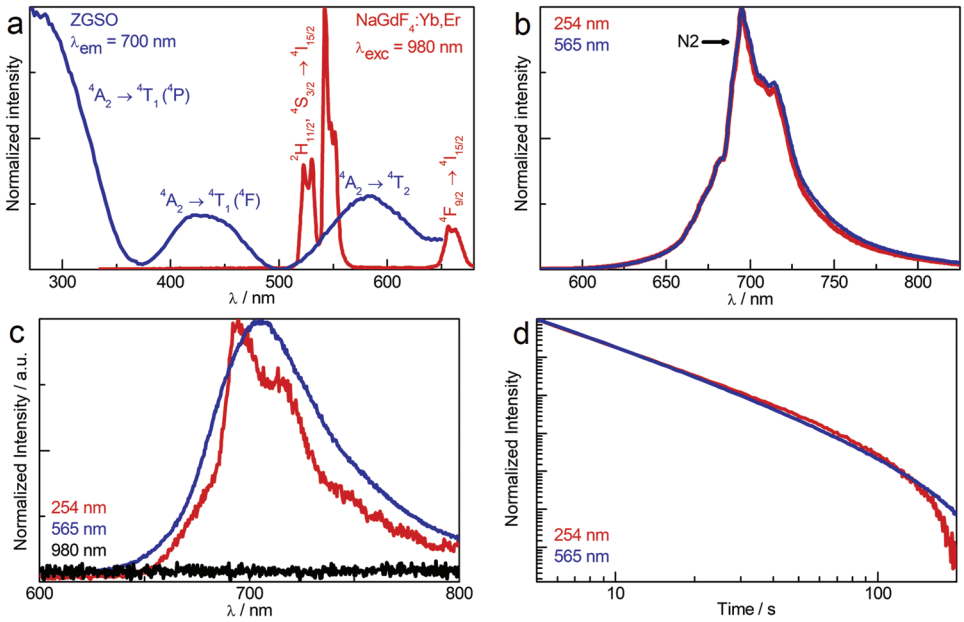

Figure 2. a) Overlap between ZGSO excitation spectrum and $NaGdF_4$:Yb, Er upconversion spectrum. b) ZGSO photoluminescence under 254 and 565 nm excitations (see Figures S5 and S6, Supporting Information, for complements). c) Persistent emission of ZGSO:Cr^{3+} 10 s after excitation stops with excitation at 254, 565, and 980 nm. The normalization in the 980 nm excitation was done according to the background of the emission spectrum with 565 nm excitation just to show the absence of signal, monochromator slits are 0.1 mm for 254 nm and 1 mm for 565 and 980 nm. d) Normalized persistent luminescence over time for ZGSO:Cr^{3+} under 254 and 565 nm excitations.

excitation remains the N2 band, as observed for micrometric size ZGSO compounds.[26] The nanosized compounds, in comparison to the bulk ZGSO, has a larger contribution from the broad $^4T_2 \rightarrow {}^4A_2$ emission band (Figure S6, Supporting Information). It appears that the excitation at 565 nm can effectively charge the persistent luminescence. This was further confirmed by the integrated persistent luminescence over time, as shown in Figure 2d even if the persistent luminescence under 565 nm remains smaller in intensity than under 254 nm excitation.

After associating by the dry impregnation method these persistent nanoparticles with $NaGdF_4$:Yb,Er nanoparticles, the optical spectroscopy properties were reinvestigated. At first, the optimal phosphors ratio was determined. Ratios ranging between 1/3, 1/1, and 3/1 for the ZGSO and $NaGdF_4$, respectively, were tested (see Figure S7, Supporting Information), and it clearly appears that the 1/1 ratio is the most efficient in terms of persistent luminescence intensity. Then in the following part of the study only the 1:1 ratio is used for the hybrid compounds associated by dry impregnation. Under excitation at 254 and 565 nm, as expected, no changes in photoluminescence and persistent luminescence shapes were found for the mixed compounds. When charging the $NaGdF_4$/ZGSO NPs with 980 nm NIR excitation (**Figure 3**a), it was possible to observe a visible and broad 700 nm emission by upconversion mechanisms. Comparing this emission with the single fluoride particles, the spectrum presents a broadband with weak intensity corresponding to a shoulder in the deep red range >650 nm and extending toward 700 nm. This emission corresponds to Cr^{3+} emission fed by the energy transfer. This result demonstrates the capability of exciting the hybrid material in the near infrared (980 nm) and with emission in the deep red (> 650 nm) arising from Er^{3+} and Cr^{3+}, both localized into the biological window.[35] This could allow further applications in the bioimaging field. The kinetics are furthermore strongly affected

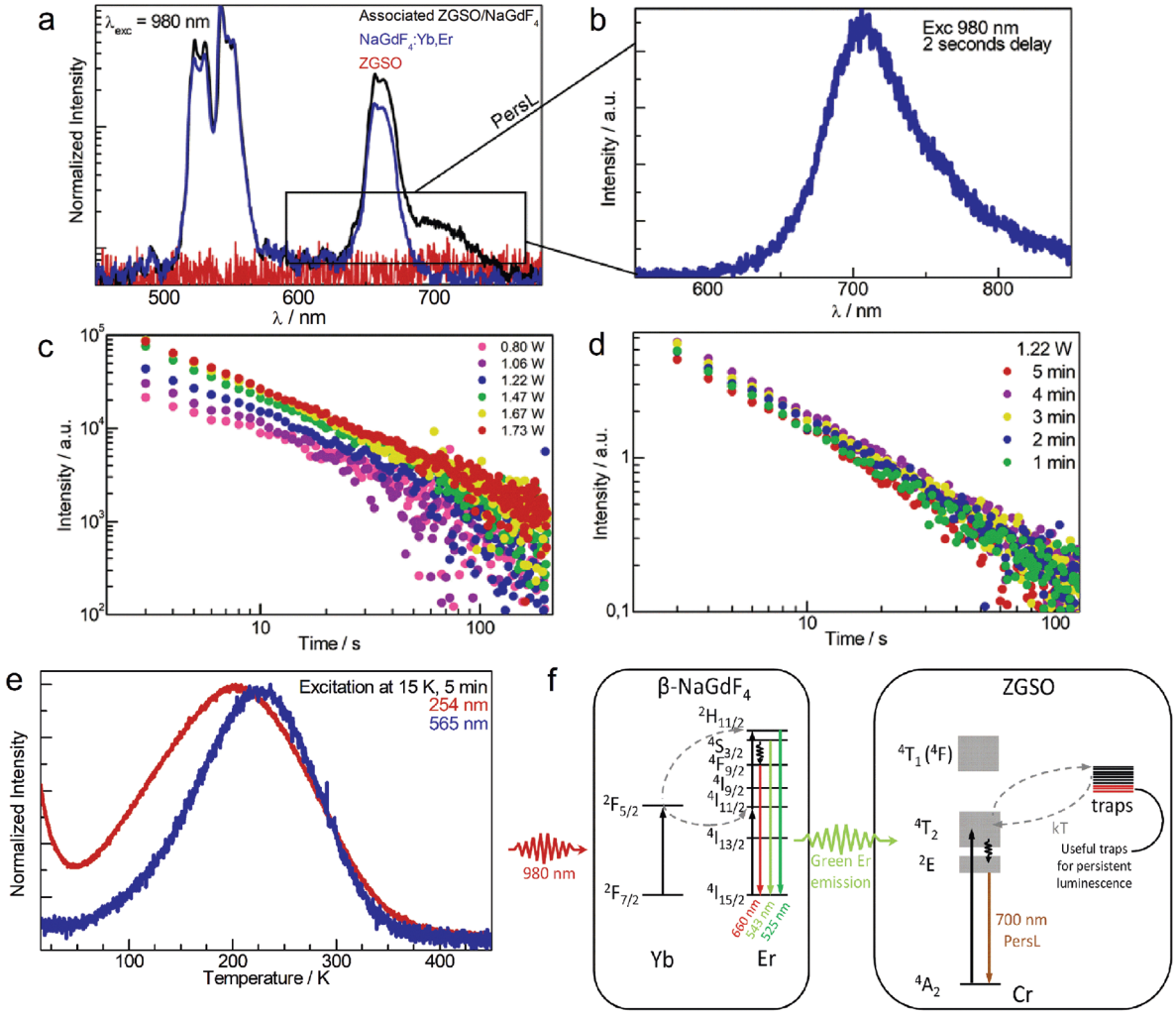

Figure 3. a) Normalized upconversion spectrum of $NaGdF_4$:Yb,Er (in blue), $NaGdF_4$ associated to ZGSO (in black), and pure ZGSO (in red). (Normalization with pure ZGSO is in the range of 0 to 0.015 to show the lack of signal). b) Persistent luminescence of $NaGdF_4$-associated ZGSO, starting 2 s after the end of excitation at 980 nm. c) Persistent luminescence of $NaGdF_4$-associated ZGSO with different charging powers using a 980 nm laser source. d) Persistent luminescence of $NaGdF_4$-associated ZGSO changing the charging time with a 980 nm laser source. e) Thermoluminescence (TSL) of $NaGdF_4$-associated ZGSO with excitations in 254 and 565 nm at 15 K. f) Proposed mechanism of the infrared excitation and emission of $NaGdF_4$-associated ZGSO nanoparticles.

by the energy transfer process, as investigated in the following part of the paper.

In Figure 3c, the associated $NaGdF_4$/ZGSO materials were excited by the 980 nm laser diode for 5 min with different excitation powers to corroborate the capability of the infrared excitation to promote the persistent luminescence. Indeed, higher excitation powers increase the duration of the persistent luminescence as seen in Figure 3c to reach several tens of seconds. This suggests that higher powers open the path to enhance the filling of traps useful for the persistent luminescence. As in the persistent luminescence mechanism, the charging time could play an important role, this was also investigated within this work and the results are presented in Figure 3d. There is no significant variation when charging from 1 to 5 min for a given 980 nm NIR power. At 15 s and 30 s charging time durations (see Figure S11, Supporting Information) the charging efficiency is however smaller. Comparing these data with the variations reported in Figure 3c when incident power is modified, this suggests that for charging times of at least 1 min, the number of filled traps only varies with the excitation power of the NIR 980 nm laser diode, but not with the duration of the excitation. Nevertheless, in the case of the bioimaging application low NIR power was mainly used, namely 0.25 W NIR laser diode, in order to limit the heating processes of the laser on the biological tissues.

Thermoluminescence (TSL) study of the mixed associated particles was performed using different excitation wavelengths at 565 and 254 nm at low temperature (15 K) to see if there is a difference in the trapping process by changing the incident wavelengths (Figure 3e). Excitation at 254 nm induced more efficient trapping than at 565 nm, with a broad band in both cases in the thermoluminescence glow curves. For excitation at 254 nm, the thermoluminescence signal peaks at 210 K and extends until 350 K, in the persistent luminescence range. It is possible to observe with the signal to noise ratio that the TSL glow curve is much more intensive after 254 nm excitation.[13] Most of the traps in this material are not located in the temperature range for good persistent luminescence, rather corresponding to effective charging at lower temperatures than room temperature. The excitation at 565 nm leads to a small shift toward higher temperatures peaking at ≈230 K. These traps should be indeed charged when exciting with 980 nm wavelength. Thermoluminescence using 980 nm as excitation wavelength was also performed, but no trapping was further observed. This suggests that the energy transfer is not efficient at low temperatures and Cr^{3+} excitation bands tend to be narrower because of the low phonon effect at 15 K.

With all this information, one can propose a mechanism for the persistent luminescence process in these materials after 980 nm excitation, as seen in Figure 3f. When 980 nm laser excitation is used, Yb^{3+} cations are excited and energy transfer to Er^{3+} within a two-photon process is observed in $NaGdF_4$ NPs. The light emitted from Er^{3+} in the green range could then further excite Cr^{3+} in ZGSO through the $^4A_2 \rightarrow {}^4T_2$ transition. From this Cr^{3+} excited state, energy transfer to traps could occur. Notice that without Cr^{3+} there is no persistent luminescence in $NaGdF_4Yb^{3+}$, Er^{3+}/ZGSO NPs. During thermal stimulation, traps are released into the system over time to reach the Cr^{3+} recombination centers, then returning to ground state through $^2E \rightarrow {}^4A_2$ transition. Due to the low energy of the green Er^{3+} emission, the trapping/de-trapping mechanism in ZGSO:Cr^{3+} should be very similar to the one previously described by Bessière et al. for ZGO:Cr^{3+}.[48] The Sn^{4+} substitution only increase the amount of site distortion namely related to anti-site defects,[28] which are very important for these low-energy excitation in ZGSO, and appears crucial for UCPL using the $NaGdF_4$/ZGSO system.

It is important to further notice that to well observe upconversion charging process, the materials should be kept away from ambient, sunlight, and photostimulation processes.[17,49]

After these optical characterizations, the $NaGdF_4$-associated ZGSO particles were first tested in a simple test to check if the persistent luminescent light emitted by the composite could be captured by a visible camera through a 2 mm-thick layer of ham. In these studies, ham was used to mimic a biological environment. The results obtained using three different excitation sources (a 254 nm lamp, an orange/red visible LED with a cut-off filter at 515 and a 980 nm diode laser) are shown in **Figure 4**. The setup for the experiments is described in Figure 4a. When using the 254 nm lamp or the visible LED, excitation was performed without the ham layer, and photons are collected after the sample holder was covered by a ham layer (direct excitation). When using the 980 nm laser, two experiments were tested: one as described with the 254 nm lamp and the visible LED, where the sample is directly excited by the excitation source before being covered by ham (Figure 4a, top), and a second one, where the excitation occurs through the ham layer (Figure 4a, bottom).

Through Figure 4b–d it is possible to see that all excitation sources were able to charge the particles allowing emitting light at ≈700 nm in the deep red through the ham layer. The infrared light excitation, namely 980 nm, was also able to excite even through the ham as shown in Figure 4e. Figure 4f shows the persistent luminescent decay profiles of $NaGdF_4$-associated ZGSO with all used excitation sources. The infrared excitation of the persistent luminescent compounds, which depends on the energy transfer from $NaGdF_4$:Yb, Er to ZGSO:Cr^{3+} is about two orders of magnitude less intensive than the direct excitation of ZGSO in the UV (band gap) or in the green/orange ($^4A_2 \rightarrow {}^4T_2$ excitation), however, it is possible to record signal for at least 5 min using a low energy light source.

After these tissue-like mimicking experiments, and before performing more complicated in vivo experiments, the ability of the associated nanocomposite to keep on emitting light in water, after 980 nm laser excitation, has been evaluated. For this purpose, two conditions have been tested in which the associated nanocomposites (16 mg $NaGdF_4$:Yb, Er/ZGSO:Cr^{3+}, 1/1 weight ratio) in an Eppendorf tube were either directly in contact with 1 mL of water (Figure S8a, Supporting Information), or the associated nanocomposite were isolated from water by confinement in a capsule, Figure S8b (Supporting Information). In these conditions, without dispersion, as can be seen in Figure S8 (Supporting Information), persistent luminescence signals can be obtained. In both cases, water reduces the intensity of the signal compared to solvent free experiments (blue

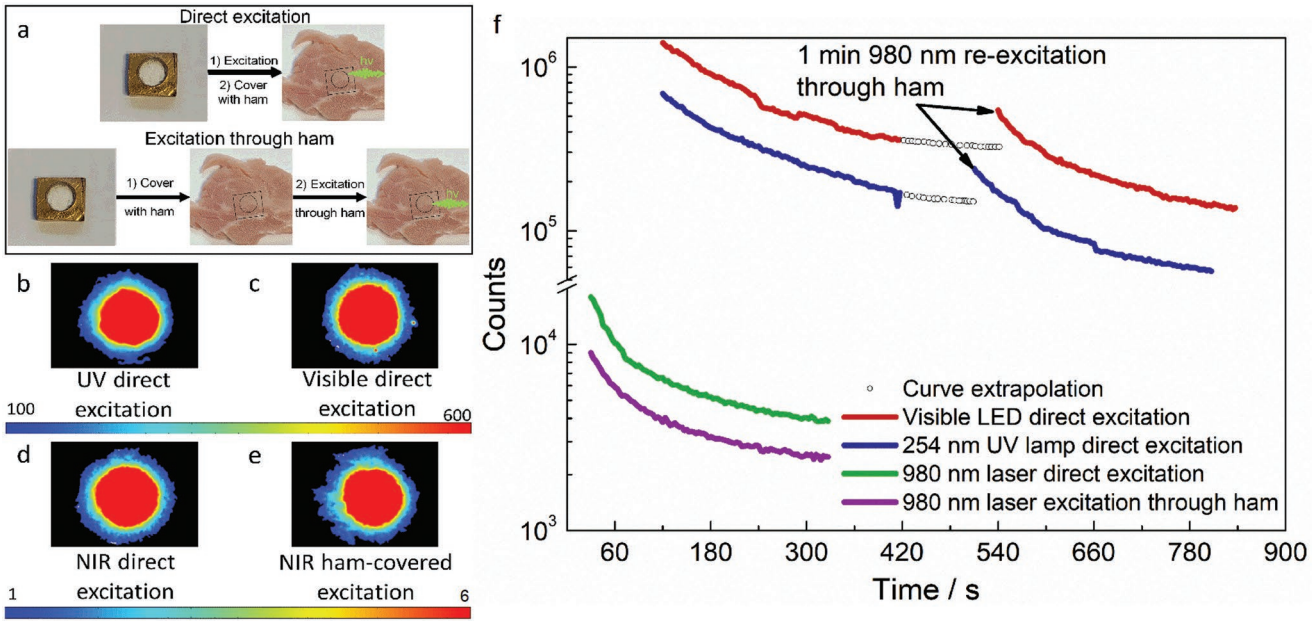

Figure 4. a) Setup used for tissue-like persistent luminescence imaging b–e) Light collected through 2 mm ham layer with $NaGdF_4$-associated ZGSO samples after excitation with: (b) 254 nm (2.1 mW cm^{-2}) for 2 min; (c) visible, orange-red LED (31.2 mW cm^{-2}) for 10 s with 515 nm cut-off filter; (d) 980 nm (5.1 W cm^{-2}) for 2 min with direct excitation of sample; (e) 980 nm (5.1 W cm^{-2}) for 2 min with excitation through the ham layer. f) Persistent luminescence decays of the four excitation schemes used in this first study.

curves, Figure S8, Supporting Information). However, when both conditions (free powder or inside a capsule) are dispersed into water, only the condition in which the associated powder has been introduced into a capsule allowed keeping a persistent luminescence signal (Figure S9, Supporting Information). This special packaging, using the associated nanocomposite inside a capsule, has been used for the in vivo experiments on mice.

Two kinds of in vivo experiments have been performed on mice. In the first series, a capsule containing the associated nanocomposite (16 mg) was excited ex situ with the 980 nm laser for 2 min (**Figure 5**a), and the excited capsule was immediately implanted in the back of a Balb/c mice, just under the skin. After observation with a ICCD camera (Biospace lab) a persistent luminescence signal, characteristic of ZGSO:Cr, was clearly detectable (Figure 5b), with an emission lasting for >5 min (Figure 5c). When there was no more signal, we have shown that it is possible to re-excite the capsule, inside the animal body (Figure 5d), allowing to recover the persistent signal (Figure 5e,f). Even if lower than after the ex situ excitation, the signal intensity is still higher than the background (BKG, black line). We have shown, that by adjusting the power of the laser (from 0.8 to 2.4 A corresponding to 1 to 5.1 W cm^{-2}) the intensity of the emitted signal can be increased to facilitate the detection (Figure 5g–i).

In a second series of experiments, we have demonstrated that it is possible to perform in vivo imaging in deeper tissue, using another way of administration of the capsule, the oral route (Figure 5j–l; Figure S10. Supporting Information). As before, the capsule can be pre-excited ex situ (Figure S10a, Supporting Information), then administered orally via a cannula and the signal emitted by the capsule can be clearly detectable (Figure S10b,c, Supporting Information). As before, when the signal is off, we have shown that it is possible to re-excite the associated composite, through the throat (Figure 5j), using a 980 nm excitation (1 W cm^{-2}, 2 min), allowing recovering the characteristic persistent signal of ZGSO:Cr (Figure 5k,l).

These in vivo results, the first realized in mice using associated UCNP/ZGSO nanocomposites highlight the feasibility of this strategy based on the emission of a persistent luminescence signal after an energy transfer mechanism. Using this phenomenon, different applications can be envisioned: after a local injection to follow the stability of an implant or the release of a drug; and after oral administration, to study the kinetic of the degradation of the capsule in the stomach.

3. Conclusions

In this work, at first, we successfully synthesized and characterized ZGSO:Cr^{3+} NPs, elaborated using a hydrothermal method. These nanoparticles present persistent luminescence with emission at ca. 700 nm ($^2E \rightarrow {}^4A_2$ transition) when excited at 254 nm and 565 nm, and indeed the excitation in the visible range is enhanced in the Sn-substituted compound. The capability of sensitization in the 565 nm Cr^{3+} band can be used to charge the persistent luminescence materials through upconversion using a fluoride host presenting high upconversion efficiency. 565 nm Cr^{3+} absorption band is particularly favorable thanks to a good overlap with Er^{3+} emission ($^4S_{3/2}$,$^2H_{11/2} \rightarrow {}^4I_{15/2}$ transitions). A core–shell system would be ideal to work with a UCPL system due to the reduced losses in energy transfer caused by distances, however, this requires a fine control of the material chemistry and leads to expensive compounds. In the present work, an alternative strategy was used in which ZGSO:Cr^{3+} NPs were associated with $NaGdF_4$:Yb^{3+}, Er^{3+} NPs, by using a

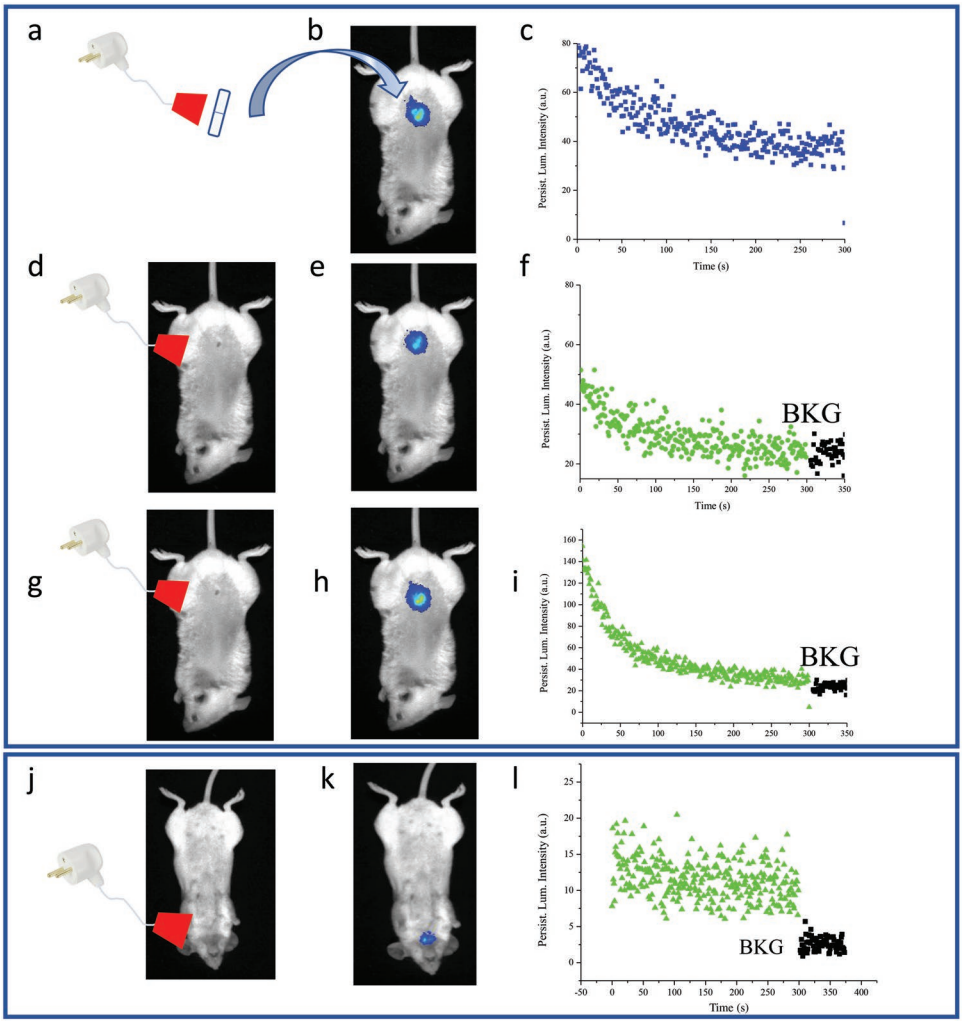

Figure 5. In vivo imaging using associated nanocomposite in capsules. a) Ex situ excitation of a capsule filled with the associated nanocomposite using 980 nm laser (1 W cm^{-2}, 2 min). b) Total counts collected after the capsule has been implanted on the back of a mice. c) Persistent luminescence decay of the capsule implanted under the skin. d) In situ re-excitation of the capsule implanted under the skin using the 980 nm laser (1 W cm^{-2}, 2 min). e) Total counts after in situ re-excitation. f) Persistent luminescence decay of the capsule re-excited in situ. g) In situ re-excitation of the capsule using the 980 nm laser (5.1 W cm^{-2}, 2 min). h) Counts of the in situ re-excited capsule. i) Persistent luminescence decay of the capsule in situ re-excited. j) In situ excitation of a capsule (40 mg) after oral administration in the throat of a mice, using the 980 nm laser (1 W cm^{-2}, 2 min). k) Counts obtained after in situ excitation of the capsule. l) Persistent luminescence decay of the in situ re-excited capsule.

fast and easy dry impregnation method. These associated particles $NaGdF_4$:Yb, Er/ZGSO:Cr showed persistent luminescence when excited with a 980 nm laser diode thanks to energy transfer from upconversion excited Er^{3+} to Cr^{3+}. Further, note that other rare earth cations (Yb^{3+}/Tm^{3+} for instance) could also be considered to reach 254 nm by upconversion (with a four-photon process), however, the use of high energy can be detrimental for in vivo applications and cell viability.

The temperature-assisted nature of this energy transfer is demonstrated by an absence of thermoluminescence glow signal when excited at 15 K with 980 nm excitation light, while direct excitation of ZGSO using a 254 or 565 nm excitation sources has intense glow signal. A mechanism is proposed for the near infrared 980 nm excitation inducing upconversion in the $NaGdF_4$:Yb, Er NPs then followed by energy transfer between excited Er^{3+} and Cr^{3+} in ZGSO NPs. After this energy transfer, defects in the ZGSO:Cr^{3+}, NPs, namely antisite defects, are filled by excited Cr^{3+} and are thermally released in the Cr^{3+} recombination centers with emission in the deep red range.

The excitation (980 nm) and emission (ca. 700 nm) wavelengths of this hybrid material are both located inside the biological window (BW-I), which allows its potential as a rechargeable persistent bioimaging probe. As demonstrated within this work, in vivo imaging is possible using pre-excited capsules loaded with a 1/1 ratio of $NaGdF_4$:Yb, Er/ ZGSO:Cr NPs, either after subcutaneous or oral administration in mice. In both cases, when the signal is off, it is possible to recover it by a re-stimulation in situ, through biological tissues. This way of imaging, based on energy transfer using laser excitation can be of particular interest in different applications, for example, to follow the stability of an implant or on the contrary to study the kinetic of degradation of the capsule. Even if a little more

difficult to synthesize, monohybrids containing $NaGdF_4$:Yb, Er, and ZGSO:Cr NPs incorporated into a silica matrix can be considered, allowing others in vivo applications after functionalization and intravenous injection.[50,51]

4. Experimental Section

β-NaGdF$_4$:Yb, Er Synthesis: To synthesize β-$NaGdF_4$:Yb, Er nanoparticles, 2.4 mL of a 0.4 mol L^{-1} $GdCl_3$ aqueous solution, 0.51 mL of a 0.4 mol L^{-1} $YbCl_3$ aqueous solution and 0.09 mL of a 0.4 mol L^{-1} $ErCl_3$ aqueous solution were mixed together in a 250 mL three-necked round flask. To the same flask, 21 mL of 1-octadecene (technical grade, Sigma–Aldrich) and 9 mL of oleic acid (analytical grade, LabSynth) were added and then, under Ar atmosphere, heated to 160 °C for 40 min and then cool down to room temperature.

During the cooling, a mixture of 0.120 g of NaOH (analytical grade, LabSynth) and 0.1776 g of NH_4F (analytical grade, LabSynth) were dissolved in 15 mL of methanol (analytical grade, LabSynth) and then added to the three-necked flask and stirred for 30 min at room temperature. Then under an argon atmosphere, the mixture was heated to 300 °C for 90 min. After the flask returns to room temperature, 10 mL of absolute ethanol was slowly added and transferred to a centrifuge tube and centrifuged for 8 min at 4400 rpm and then the supernatant was removed. The material was centrifuged six more times, each time adding 5 mL of absolute ethanol, followed by removal of the supernatant. After the last centrifugation the remaining ethanol is evaporated, and the β-$NaGdF_4$:Yb, Er solid was used for analysis and characterizations.

ZGSO Synthesis: The synthesis of ZGSO was adapted from the synthesis of ZGO nanoparticles by a hydrothermal method,[13] the tin concentration was chosen according to the results from Pan et al.[28] In this method, 8.94 mmol of gallium oxide (99.999%, Alfa Aesar) were dissolved in 10 mL of concentrated nitric acid (35 wt%) under hydrothermal conditions for 48 h at 150 °C. Then 10 mL of an aqueous solution containing 17.82 mmol of zinc nitrate hexahydrate (>99%, Fluka), 4.42 mmol tin (IV) chloride pentahydrate (98%, Alfa Aesar), and 0.07 mmol chromium (III) nitrate nonahydrate (99.9%, Alfa Aesar) were added to the vessel under vigorous stirring. The solution pH was adjusted to 7.5 using ammonia solution (30 wt%), was stirred for 3 h at room temperature and then transferred to a stainless-steel autoclave, in which it was kept for 24 h at 120 °C. The resulting solid was washed several times with water and ethanol and then dried at 60 °C for 2 h, and was sintered in air at 750 °C for 2 h in a tubular oven. The obtained white powder was then ground in hydrochloric acid (5 mmol L^{-1}), stirred overnight in HCl 50 mM, and centrifuged at 4500 rpm for 10 min, selecting the supernatant that had an average size of ≈100 nm, as seen in Figure S3 (Supporting Information).

Dry Impregnation: An amount of 90 mg of ZGSO was collected from the former suspension by a centrifugation at 14500 rpm, then the pellet was dried under vacuum for 2 h at 60 °C and the solid was spread on the Petri dish heated at 50 °C. To this Petri dish, 5 mL of a suspension, containing 90 mg of $NaGdF_4$ in cyclohexane, was added in 100 µL aliquotes by spreading it over the ZGSO and mixing the ZGSO powder and $NaGdF_4$ suspension until the mixture was dry, repeating this process until all $NaGdF_4$ suspension is added. The obtained $NaGdF_4$ mixed with ZGSO was then used for analysis in solid state.

Characterization: The crystal structure and phase analysis were performed by powder X-Ray diffraction in a PANanalytical X'Pert Pro diffractometer using Cu Kα radiation operating at 40 mA and 40 kV in a 2θ range from 10 to 70°, with a scanning step of 0.0167°. TEM images are taken using a Tecnai G2 Spirit Apparatus and the images are recorded on a CCD camera (Orius Gatan 832 Digital). Carbon-coated copper TEM grids are used after evaporation of one drop of aqueous nanoparticles suspension. Excitation and emission spectra of ZGSO nanoparticles are registered with a Cary Eclipse Varian spectrophotometer in phosphorescence mode, ranging from 250 to 650 nm excitation for the emission band at 700 nm. Other optical measurements were recorded using a charge-coupled hyperspectral camera (Roper Pixis 100) coupled to a visible monochromator (Acton Spectra Pro with grating 300 grooves per mm, Princeton Instruments) using the suitable excitation source to the measurement. For these experiments, as excitation sources and wavelength, a 6 W 254 nm Hg UV lamp, a 565 nm 1 W LED (Thorlabs) or a 980 nm (LIMO), powers 0.6–2.2 W were used.

Tissue-Like Experiments Realized on Ham Slices: To simulate biological tissues, experiments were done using ham bought in a supermarket. For this purpose, 30 mg of samples in powder form (ZGSO + $NaGdF_4$) were deposited in a sample holder and observed with an Optima camera (Biospace Lab, France). The sample holder was covered by a 2 mm thick pork ham layer during data collection in all cases. For the excitation, three different sources were used: i) a 6 W 254 nm Hg UV lamp (irradiance 2.1 mW cm^{-2}), ii) a 70 W 5700 lm LED lamp (irradiance 31.2 mW cm^{-2}) equipped with 515 nm cut-off filter, or iii) a 980 nm (irradiance between 1 and 5.1 W cm^{-2}) diode laser.

For the infrared diode laser excitation experiments, two different methods were used: i) Without the ham layer over the sample holder, the powders were excited for 2 min by the infrared laser. After excitation, the ham was readily put to cover the sample holder before decay data collection, starting data collection 30 s after the excitation stopped. ii) With the ham layer already covering the sample holder, the powders were excited for 2 min using the infrared laser, simulating an in vivo excitation through biological tissue. The decay data collection also started 30 s after the excitation ceased.

For the visible LED lamp excitation, the sample was excited for 10 s without the ham layer, which was then put over the sample holder. Data collection started 2 min after excitation ceased to avoid camera saturation. After 5 min of decay data collection, the sample was re-excited for 1 min through the ham layer using the 980 nm infrared diode laser to recharge persistent luminescence, simulating an in vivo re-excitation of the sample, and decay data was then re-collected for more 5 min.

For the UV lamp excitation, the sample was excited for 2 min without the ham layer, which was then added to cover the sample holder. Decay data collection started 2 min after the end of the excitation to avoid camera saturation. After 5 min of data collection, the sample was re-excited for 1 min using the 980 nm infrared diode laser through the ham layer to recharge persistent luminescence. After the re-excitation, the decay data was collected for 5 min.

In Vivo Experiments on Mice: All experiments involving the mice were approved by French Comité d'éthique en expérimentation animale No. 034 and by French Ministry of Research APAFIS#8519-20 16090514387844. Local administration route: capsule containing 16 mg of nanocomposite (1:1 ratio) are first excited ex situ for 2 min at 980 nm (1 W cm^{-2}) and implanted under the skin of a five-week-old female BALB/c mice (Janvier) anaesthetized by intraperitoneal injection of ketamine/xylazine. The persistent luminescence signal was then collected for 5 min with a Biospace camera. After ≈15 min, in situ re-excitation of the capsule was performed for 2 min at 980 nm (1 W cm^{-2}) and the decay signal was recorded for 5 min.

Oral administration route: a capsule containing 40 mg of nanocomposite (1:1 ratio) was first excited ex situ for 2 min at 980 nm (1 W cm^{-2}) then administered to the throat of a five-week-old anaesthetized female BALB/c mice, via a cannula, and decay data was collected for 5 min. After ≈15 min, in situ re-excitation of the capsule was realized by using the infrared diode laser (1 W cm^{-2}) for 2 min, and then the decay data was collected for 5 min. Time duration effect of the excitation is reported in Figure S11 (Supporting Information).

Supporting Information

Supporting Information is available from the Wiley Online Library or from the author.

Acknowledgements

L.G. wants to acknowledge CAPES (Coordenação de Aperfeiçoamento de Pessoal de Nível Superior) for a scholarship grant (#88887.371146/2019-00) and CNPq (141252/2017-0). L.C.V.R. acknowledges FAPESP for funding (2018/05280-5; CNPQ #315126/2021-3). ANR PERSIST #18-CE0-8-0012 France is acknowledged for funding the project.

Conflict of Interest

The authors declare no conflict of interest.

Data Availability Statement

The data that support the findings of this study are available from the corresponding author upon reasonable request.

Keywords

energy transfer, in vivo imaging, nanoparticles, persistent luminescence, upconversion, upconverted persistent luminescence

Received: June 24, 2022
Revised: November 13, 2022
Published online: January 18, 2023

[1] P. Xiong, M. Peng, *J. Mater. Chem. C* **2019**, *7*, 8303.
[2] M. Lastusaari, T. Laamanen, M. Malkamäki, K. O. Eskola, A. Kotlov, S. Carlson, E. Welter, H. F. Brito, M. Bettinelli, H. Jungner, J. Hölsä, *Eur. J. Mineral.* **2012**, *24*, 885.
[3] J. Xu, S. Tanabe, *J. Lumin.* **2019**, *205*, 581.
[4] T. Matsuzawa, Y. Aoki, N. Takeuchi, Y. Murayama, *J. Electrochem. Soc.* **1996**, *143*, 2670.
[5] K. Van den Eeckhout, D. Poelman, P. Smet, *Materials* **2013**, *6*, 2789.
[6] K. Van Den Eeckhout, P. F. Smet, D. Poelman, *Materials* **2010**, *3*, 2536.
[7] Y. Zhuang, Y. Katayama, J. Ueda, S. Tanabe, *Opt. Mater.* **2014**, *36*, 1907.
[8] Y. Li, M. Gecevicius, J. Qiu, *Chem. Soc. Rev.* **2016**, *45*, 2090.
[9] J. Xu, D. Murata, J. Ueda, B. Viana, S. Tanabe, *Inorg. Chem.* **2018**, *57*, 5194.
[10] J. Xu, J. Ueda, Y. Zhuang, B. Viana, S. Tanabe, *Appl. Phys. Express* **2015**, *8*, 042602.
[11] A. Bessière, A. Lecointre, R. A. Benhamou, E. Suard, G. Wallez, B. Viana, *J. Mater. Chem. C* **2013**, *1*, 1252.
[12] D. Van der Heggen, J. J. Joos, A. Feng, V. Fritz, T. Delgado, N. Gartmann, B. Walfort, D. Rytz, H. Hagemann, D. Poelman, B. Viana, P. F. Smet, *Adv. Funct. Mater.* **2022**, *32*, 2208809.
[13] T. Maldiney, A. Bessière, J. Seguin, E. Teston, S. K. Sharma, B. Viana, A. J. J. Bos, P. Dorenbos, M. Bessodes, D. Gourier, D. Scherman, C. Richard, *Nat. Mater.* **2014**, *13*, 418.
[14] Q. Luo, W. Wang, J. Tan, Q. Yuan, *Chin. J. Chem.* **2021**, *39*, 1009.
[15] T. Lécuyer, E. Teston, G. Ramirez-Garcia, T. Maldiney, B. Viana, J. Seguin, N. Mignet, D. Scherman, C. Richard, *Theranostics* **2016**, *6*, 2488.
[16] J. Liu, T. Lécuyer, J. Seguin, N. Mignet, D. Scherman, B. Viana, C. Richard, *Adv. Drug Delivery Rev.* **2019**, *138*, 193.
[17] S. K. Sharma, D. Gourier, E. Teston, D. Scherman, C. Richard, B. Viana, *Opt. Mater.* **2017**, *63*, 51.
[18] C. Richard, B. Viana, *Light Sci Appl* **2022**, *11*, 123.
[19] H. F. Brito, J. Hölsä, T. Laamanen, M. Lastusaari, M. Malkamäki, L. C. V. Rodrigues, *Opt. Mater. Express* **2012**, *2*, 371.
[20] L. C. V. Rodrigues, J. Hölsä, M. Lastusaari, M. C. F. C. Felinto, H. F. Brito, *J. Mater. Chem. C* **2014**, *2*, 1612.
[21] F. Liu, Y. Chen, Y. Liang, Z. Pan, *Opt. Lett.* **2016**, *41*, 954.
[22] V. Castaing, A. D. Sontakke, A. J. Fernández-Carrión, N. Touati, L. Binet, M. Allix, D. Gourier, B. Viana, *Eur. J. Inorg. Chem.* **2017**, *2017*, 5114.
[23] Y. Chen, F. Liu, Y. Liang, X. Wang, J. Bi, X. J. Wang, Z. Pan, *J. Mater. Chem. C* **2018**, *6*, 8002.
[24] F. Liu, Y. Liang, Z. Pan, *Phys. Rev. Lett.* **2014**, *113*, 177401.
[25] Y. Cheng, K. Sun, P. Ge, *Opt. Mater.* **2018**, *83*, 13.
[26] Z. Li, L. Huang, Y. Zhang, Y. Zhao, H. Yang, G. Han, *Nano Res.* **2017**, *10*, 1840.
[27] L. Hu, Y. Fan, L. Liu, X. Li, B. Zhao, R. Wang, P. Wang, A. M. El-Toni, F. Zhang, *Adv. Opt. Mater.* **2017**, *5*, 1.
[28] Z. Pan, V. Castaing, L. Yan, L. Zhang, C. Zhang, K. Shao, Y. Zheng, C. Duan, J. Liu, C. Richard, B. Viana, *J. Phys. Chem. C* **2020**, *124*, 8347.
[29] S. P. Tiwari, S. K. Maurya, R. S. Yadav, A. Kumar, V. Kumar, M.-F. Joubert, H. C. Swart, *J. Vac. Sci. Technol. B* **2018**, *36*, 060801.
[30] P. Ramasamy, P. Chandra, S. W. Rhee, J. Kim, *Nanoscale* **2013**, *5*, 8711.
[31] W. H. Tse, L. Chen, C. M. McCurdy, C. M. Tarapacki, B. A. Chronik, J. Zhang, *Can. J. Chem. Eng.* **2019**, *97*, 2678.
[32] C. Liu, Z. Gao, J. Zeng, Y. Hou, F. Fang, Y. Li, R. Qiao, L. Shen, H. Lei, W. Yang, M. Gao, *ACS Nano* **2013**, *7*, 7227.
[33] G. Ramírez-García, S. Gutiérrez-Granados, M. A. Gallegos-Corona, L. Palma-Tirado, F. d'Orlyé, A. Varenne, N. Mignet, C. Richard, M. Martínez-Alfaro, *Int. J. Pharm.* **2017**, *532*, 686.
[34] T. Lécuyer, J. Seguin, A. Balfourier, M. Delagrange, P. Burckel, R. Lai-Kuen, V. Mignon, B. Ducos, M. Tharaud, B. Saubaméa, D. Scherman, N. Mignet, F. Gazeau, C. Richard, *Nanoscale* **2022**, *14*, 15760.
[35] A. M. Smith, M. C. Mancini, S. Nie, *Nat. Nanotechnol.* **2009**, *4*, 710.
[36] T. Lécuyer, M. A. Durand, J. Volatron, M. Desmau, R. Lai-Kuen, Y. Corvis, J. Seguin, G. Wang, D. Alloyeau, D. Scherman, N. Mignet, F. Gazeau, C. Richard, *Nanoscale* **2020**, *12*, 1967.
[37] Y. Li, S. Zhou, Y. Li, K. Sharafudeen, Z. Ma, G. Dong, M. Peng, J. Qiu, *J. Mater. Chem. C* **2014**, *2*, 2657.
[38] W. Jiang, L. Huang, F. Mo, Y. Zhong, L. Xu, F. Fu, *J. Mater. Chem. B* **2019**, *7*, 3019.
[39] R. Zou, J. Huang, J. Shi, L. Huang, X. Zhang, K. L. Wong, H. Zhang, D. Jin, J. Wang, Q. Su, *Nano Res.* **2017**, *10*, 2070.
[40] E. Palo, M. Tuomisto, I. Hyppänen, H. C. Swart, J. Hölsä, T. Soukka, M. Lastusaari, *J. Lumin.* **2017**, *185*, 125.
[41] M. Pollnau, D. Gamelin, S. Lüthi, H. Güdel, M. Hehlen, *Phys. Rev. B Condens. Matter Mater. Phys.* **2000**, *61*, 3337.
[42] X. Ye, Y. Luo, S. Liu, D. Hou, W. You, *J. Alloys Compd.* **2017**, *701*, 806.
[43] C. Cheng, Y. Xu, S. Liu, Y. Liu, X. Wang, J. Wang, G. De, *J. Mater. Chem. C* **2019**, *7*, 8898.
[44] M. Back, J. Ueda, J. Xu, K. Asami, M. G. Brik, S. Tanabe, *Adv. Opt. Mater.* **2020**, *8*, 2000124.
[45] S. K. Sharma, A. Bessière, N. Basavaraju, K. R. Priolkar, L. Binet, B. Viana, D. Gourier, *J. Lumin.* **2014**, *155*, 251.
[46] P. F. Smet, K. Van Den Eeckhout, A. J. J. Bos, E. Van Der Kolk, P. Dorenbos, *J. Lumin.* **2012**, *132*, 682.
[47] P. F. Smet, K. Van den Eeckhout, O. Q. De Clercq, D. Poelman, *Persistent Phosphors*, Elsevier, Amsterdam, The Netherlands, **2015**.
[48] A. Bessière, S. K. Sharma, N. Basavaraju, K. R. Priolkar, L. Binet, B. Viana, A. J. J. Bos, T. Maldiney, C. Richard, D. Scherman, D. Gourier, *Chem. Mater.* **2014**, *26*, 1365.
[49] Y. Katayama, Y. Viana, D. Gourier, J. Xu, S. Tanabe, *Opt. Mater. Express* **2016**, *6*, 1405.
[50] E. Teston, Y. Lalatonne, D. Elgrabli, G. Autret, L. Motte, F. Gazeau, D. Scherman, O. Clément, C. Richard, T. Maldiney, *Small* **2015**, *11*, 2696.
[51] E. Teston, T. Maldiney, I. Marangon, J. Volatron, Y. Lalatonne, L. Motte, C. Boisson-Vidal, G. Autret, O. Clément, D. Scherman, F. Gazeau, C. Richard, *Small* **2018**, *14*, 1800020.